

High Internal Phase Water-in-Oil Emulsions Studied by Small-Angle Neutron Scattering

Philip A. Reynolds, Elliot P. Gilbert, and John W. White*

Research School of Chemistry, The Australian National University, Canberra ACT 0200, Australia

Received: January 27, 2000; In Final Form: April 25, 2000

We present a preliminary examination of three isotopically substituted series of concentrated emulsions by small-angle neutron scattering (SANS). These have 90% internal phase water or salt solution droplets in continuous hexadecane. The surfactants have polyisobutylene oligomer tails with mainly acid–amide headgroups. The emulsion structure is well approximated by a polydisperse system of micrometer scale aqueous spheres surrounded by a continuous, surfactant/hexadecane phase L_2 microemulsion. Even though the aqueous volume fraction in the whole emulsion is ca. 90%, we see no evidence for nonsphericity of aqueous droplets, i.e., long-scale planarity of the aqueous–hexadecane boundary. The salt emulsion data fit well to a model in which there is 12–16% of the surfactant absorbed as a monolayer at a flat (0(3) Å) aqueous–oil interface, with the remainder as spherical 26–30 Å radius reverse micelles in the hexadecane continuous oil phase. The micelles contain 8–10% water and a large fraction of hexadecane as well as the surfactant. The water emulsion has less surfactant absorbed at a much rougher (62(1) Å) aqueous interface, and larger micelles containing more water—all reflecting less tightly held water in the aqueous as opposed to salt solution droplets. The structure is insensitive to heating from 20 to 70 °C, but cooling to 5 °C precipitates large surfactant aggregates, giving three phases. The three possible relative specific surface areas (aqueous/aggregate, aggregate/hexadecane, and aqueous/hexadecane) show increasing intrusion of the surfactant aggregate into the aqueous droplets as the aggregate increases in size.

Introduction

While simple emulsions are both important and well studied by many techniques,¹ there has been little investigation by SANS to probe structure at the nanometer scale. Water-in-fluorocarbon high internal phase emulsions have been studied (see refs 2 and 3 and references therein), and there is a very recent study of a dilute oil-in-water emulsion.⁴ Microemulsions have been extensively characterized by SANS,^{5–26} and it may be that the availability of a suitable microemulsion has a bearing on the stability and ease of preparation of emulsions.^{2,3,27} In this paper we analyze the small-angle neutron scattering (SANS) from aqueous/hydrocarbon high internal phase emulsions for which the neutron scattering contrast has been varied between the components to selectively identify the scattering from different components of the emulsion structure.

Metastable emulsions can form when an aqueous solution is mixed with a surfactant/oil mixture at a temperature above the “phase inversion temperature” (PIT) or “hydrophile–lipophile balance temperature” (HLB, defined below) of the ternary phase diagram. High internal phase water-in-oil emulsions are defined as emulsions in which the volume fraction of aqueous phase droplets exceeds the 74% close-packed limit for monodisperse spheres. Such monodisperse emulsions cannot remain as spherical droplets and so exhibit flattening of the interfaces. We conventionally distinguish distinct regions of flattened membranes and Plateau borders where three or more droplets meet. For emulsions with significant polydispersity in droplet size, however, and in our 90% aqueous emulsions, droplet sizes usually vary by a factor of 5;²⁸ the volume fraction at which flattening begins increases significantly even up to 97%.²⁹ Cryo-

TEM measurements on our emulsions show that all droplets are significantly rounded, often appearing circular with, as might be expected, small droplets of ca. 1 μm occupying interstices between larger ones.²⁸ Our emulsion structure is well approximated by an assembly of polydisperse spheres, and the oil phase is the inverse—a continuous region of continually varying thickness which is locally flat on the 500 Å radius of curvature scale, but curved at a larger scale.

The SANS experiments were directed at the microstructure within the aqueous and/or oil regions, and the nature of the interface between them. Both the oil-rich and the water-rich regions are of interest. Water/surfactant/oil mixtures, often with cosurfactants, have been intensively studied by SANS and many other techniques.^{1,16,30–41} The phase behavior in normal circumstances with nonionic surfactants is now broadly understood.³⁶ This is not so for ionic and/or mixed surfactants,^{35,42,43} where other structures such as stable disks or long coiled wormlike structures may occur. For the nonionics, the oil-rich corner of the ternary phase diagram is less studied than the water-rich corner, but it does appear to be broadly symmetrical with the water-rich corner.³² In the oil-rich corner a number of phases appear in which surfactant–water entities and oil form a structure. At surfactant + water volume fractions around 0.2, there is a characteristic evolution of the phase diagram with temperature. At low temperatures (but still above the oil freezing point) a two-phase region of an isotropic oil-in-water microemulsion (L_1) is observed in equilibrium with excess oil, and this becomes at higher temperatures a single-phase L_1 region. On further increasing the temperature, a short two-phase region passes into an optically anisotropic L_α lamellar phase, and then, after the HLB is reached, the system passes through symmetric regions containing the reverse microemulsion L_2 phase—successively $L_\alpha + L_2$, L_2 , and last L_2 plus excess water. In

* To whom correspondence should be addressed. E-mail: jww@rsc.anu.edu.au. Fax: (61) 2 6249 4903.

volume fraction—temperature space this sequence forms a characteristic “fishtail” shape, as the lamellar phase becomes less favored. This sequence is understood theoretically⁴¹ in terms of the changing interfacial curvature.

The physical properties of these phases indicate aspects of their structure. As the L_2 lamellar phase is diluted with oil, the relatively high electrical conductivity changes little as we pass from lamellar L_α to reverse microemulsion L_2 . But before the next phase boundary is reached, the conductivity suddenly decreases by 10^4 or more.^{44–46} This has been interpreted as showing the existence of a percolation boundary between a water-continuous microstructure and a system of isolated micelles. This has been labeled as the boundary between an L_3 phase and an L_2 phase.

There are various models for the L_3/L_2 structures, which change due to an increase in curvature of the surfactant local structure, as the composition moves from the lamellar to the excess-water phase boundary. In the literature it is agreed that at one end there are lamellae with some small amount of interconnection, and at the other end reverse, almost-spherical micelles. From the lamellae, in the L_α phase, dilution with oil in one picture gives a bicontinuous L_3 structure (with local lamellar structure) which breaks into lamellar pieces and then into rods in the L_2 phase. The disordered open connected (DOC) model pictures this as reverse spherical micelles connected by cylindrical rods. The number of these rods diminishes as oil dilution increases, until at the percolation limit the continuous water connection is broken.⁴⁷ Computer simulations predict a steady increase in topological defects in a basically lamellar structure, but including passage defects and droplets, as oil dilution initially proceeds.³⁰

The electrical conductivity of the emulsions studied in this paper is small, at about 10 nS m^{-1} .²⁸ This is characteristic of a nonbicontinuous L_2 phase, an assignment supported by the absence of even a transient birefringence on shearing the samples. The fundamental question for an interpretation of the neutron scattering data in this region of the phase diagram is whether a rod, disk/lamellar, or spherical model is the more appropriate description of the complex situation. For related systems, monodisperse rod models provide a good fit to such data.⁵ In the oil-rich corner of the phase diagram at least one case has shown that oblate shapes are not present and that prolate, rodlike, structures fit a variety of experimental data well.³³ However, oblate structures are also known^{42,48} in mixed surfactant situations such as the present emulsion system, and cannot be entirely excluded. Another possibility, not often modeled, is markedly polydisperse spheres. We cannot even entirely exclude fully lamellar structures. In most surfactant/water/alkane ternary phase diagrams the lamellar region does not extend far into high dilutions of alkane. However, Larche et al.⁴⁰ found that they could dilute a surfactant/water/pentanol lamellar phase with a large amount of decane while still retaining the lamellar structure.

Given the previous cryo-TEM, dielectric, and optical measurements on our PIB/hexadecane/saltwater emulsion, we might suspect that SANS experiments on high internal phase water-in-oil (W/O) emulsions will give scattering patterns which might be modeled by an assembly of polydisperse spherical aqueous droplets, separated by an L_2 phase oil microemulsion containing surfactant/water reverse micellar structures. We have examined three isotopically substituted series of high internal phase water in hexadecane emulsions by SANS, one aqueous phase and two salt solutions, and have shown that this is so.

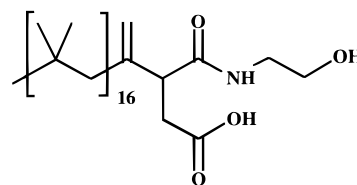


Figure 1. Typical surfactant molecule. The headgroup, carbon—carbon double bond site, degree of polymerization, and isomeric nature are all variable.

Experimental Section

Preparation of Emulsions. The surfactant, A, is prepared from polyisobutylene, PIB, average molecular weight 1110 and polydispersity M_w/M_n 1.8, with 70% exo double bond content. This is reacted with maleic anhydride and 2-hydroxyethanolamine to give the surfactant species polyisobutylene *N*-(2-hydroxyethyl)succinamide (Figure 1). The amide also contains less than 5% imide formed by slow elimination of water with cyclization from the amide. The surfactant, E, contains 45% active surfactant and 55% inactive oil and oil-soluble PIB species. The active component is similar to A but contains more disordered chains and a mixture of headgroup species. The average molecular weight is 1000, and the polydispersity M_w/M_n is 1.5.

Stock solutions of 3.62:1 w/w ammonium nitrate/deuterated water solutions were prepared and heated in a water bath at ca. 80 °C. The high temperature is necessary since this salt concentration is supersaturated at room temperature. The oil phase (*n*-hexadecane and surfactant) was preheated in a separate water bath also at ca. 80 °C while being stirred with a T-bar spindle attached to a Janke and Kunkel RW20 stirrer. The ammonium nitrate solution was added slowly over 30 s to the oil phase at a speed setting of 5 (ca. 250 rpm) to ensure emulsion formation. This was followed by rapid stirring at speed 10 (ca. 500 rpm) for 5 min while the stirrer was moved up and down through the emulsion vessel to ensure thorough mixing. This method reproducibly forms down to 10 g quantities of emulsion stable to salt crystallization at room temperature. Aqueous emulsions and those containing calcium nitrate were prepared in the same way, both using E surfactant. The emulsions contained from 1.0% to 1.3% weight fraction active surfactant and were all 90% aqueous phase, 10% oil phase.

It is useful to tabulate the scattering length densities (SLDs) and densities for the various components of our mixtures (Table 1). We have assumed a density of 1.40 g cm^{-3} for our standard mix of ca. 3.62 g of hydrogenous ammonium nitrate/g of deuterium oxide. This is derived by extrapolation of high-temperature density data for hydrogenous materials, since at 20 °C this concentration is unstable to crystallization in the bulk, although not in the emulsion.²⁸ At high temperatures the all-hydrogenous same molarity mix gives a density of $(1.38 - 0.0007T(^{\circ}\text{C})) \text{ Mg m}^{-3}$. A correction for deuteration derived from relative molecular volumes has been applied.

SANS Experiments. SANS experiments were performed on both the LOQ instrument at the Rutherford Appleton Laboratory, U.K., and the SAND instrument at the Intense Pulsed Neutron Source, Argonne National Laboratory.^{49–51}

At LOQ all samples were mounted in 1 mm thick flat quartz cells, and individual runs lasted for ca. 30 min. Five differently deuterated samples were run for three different emulsion systems: (a) $\text{D}_2\text{O}-\text{H}_2\text{O}$ mixtures/E surfactant/ $\text{C}_{16}\text{D}_{34}$ (1.3 wt % active surfactant) known as $\text{H}_2\text{O}-\text{E}$, (b) $\text{NH}_4\text{NO}_3 + \text{D}_2\text{O}/\text{E}$ surfactant/ $\text{C}_{16}\text{D}_{34}-\text{C}_{16}\text{H}_{34}$ mixtures (1.1 wt % active surfactant)

TABLE 1: Calculated Scattering Length and Physical Densities for Components of the Emulsions ($\times 10^{10} \text{ cm}^{-2}$ and g cm^{-3})

substance	neutron scattering length density	physical density	substance	neutron scattering length density	physical density
H ₂ O	-0.56	1.00	C ₁₆ D ₃₄	6.74	0.889
D ₂ O	6.36	1.11	NH ₄ NO ₃ + D ₂ O	3.52	1.40
C ₁₆ H ₃₄	-0.44	0.773	surfactant	-0.20	1.12

known as AN-E, (c) NH₄NO₃ + D₂O/A surfactant/C₁₆D₃₄–C₁₆H₃₄ mixtures (1.0 wt % surfactant) known as AN-A.

Each series was run at three temperatures, 20, 70–80, and then 5 °C. To make background corrections, water mixtures at 10, 25, 60, and 100 mol % D₂O, and ammonium nitrate dissolved to 6 M in D₂O and H₂O, were all run at 20 °C. The 100 mol % D₂O background was also run at 80 °C. The temperature dependence of the background scattering was slight, though measurable. The relative scattering scaled well with the proton scattering length density in the beam since incoherent scattering from protons dominates all the background samples (except 100% D₂O). Accordingly for all samples a background for 100% D₂O was subtracted, followed by a scaled incoherent correction of 10% D₂O minus 100% D₂O measurements adjusted by the known relative proton content of the background and sample. The error in this procedure may be estimated at 0.05 cm^{-1} , from the mutual consistency of the background data and the high Q values of the corrected sample signals. This is approximately 5% of the maximum incoherent background of 1 cm^{-1} . The data were reduced to an absolute scale by measurement of standard polystyrene blend samples. Figure 2 shows the three contrast series, run at 20 °C, while Figure 3 shows some of the temperature dependence of the SANS scattering.

At SAND, each sample in series b was run at 20 °C in 2 mm thickness cells for 4 h. After allowance for multiple scattering the SAND data and LOQ data are similar. In addition three samples prepared with calcium rather than ammonium nitrate were run. The latter were of identical composition but different in the way the emulsion was made. Sample a was made with 2 min of fast mechanical stirring after 30 s of slow stirring, sample b with 5 min of stirring after 30 s of slow stirring, and sample c with 2 min of stirring, with a more efficient stirring action after 30 s of slow stirring. The data from these samples were reduced to an absolute scale in a way similar to that of the LOQ data by use of H₂O background and standard polymer scattering samples.

Theoretical Analysis

The scattering vector, Q , is defined as the difference between the incident and scattered neutron wavevectors. For elastic scattering, $Q = |\mathbf{Q}| = (4\pi/\lambda) \sin \theta$, where 2θ is the angle through which neutrons are scattered and λ is the neutron wavelength. All fits were performed by use of interactive IGOR⁵² procedures, obtained from NIST,⁵³ but with local addition of code for worms, flat interfaces, and lamellae (see below). Theoretical intensities were corrected by convolution with the known resolution factors for LOQ⁵⁴ and SAND.⁵¹ Where necessary a small flat background has been applied in the fits to account for small errors in our incoherent background correction. These corrections are always less than 10% of the total incoherent correction. It appears that the background correction described above underestimates the incoherent background consistently by about 5%—an acceptable error.

We have modeled the unconvoluted total intensity as the sum of a contribution from a flat interface between the aqueous

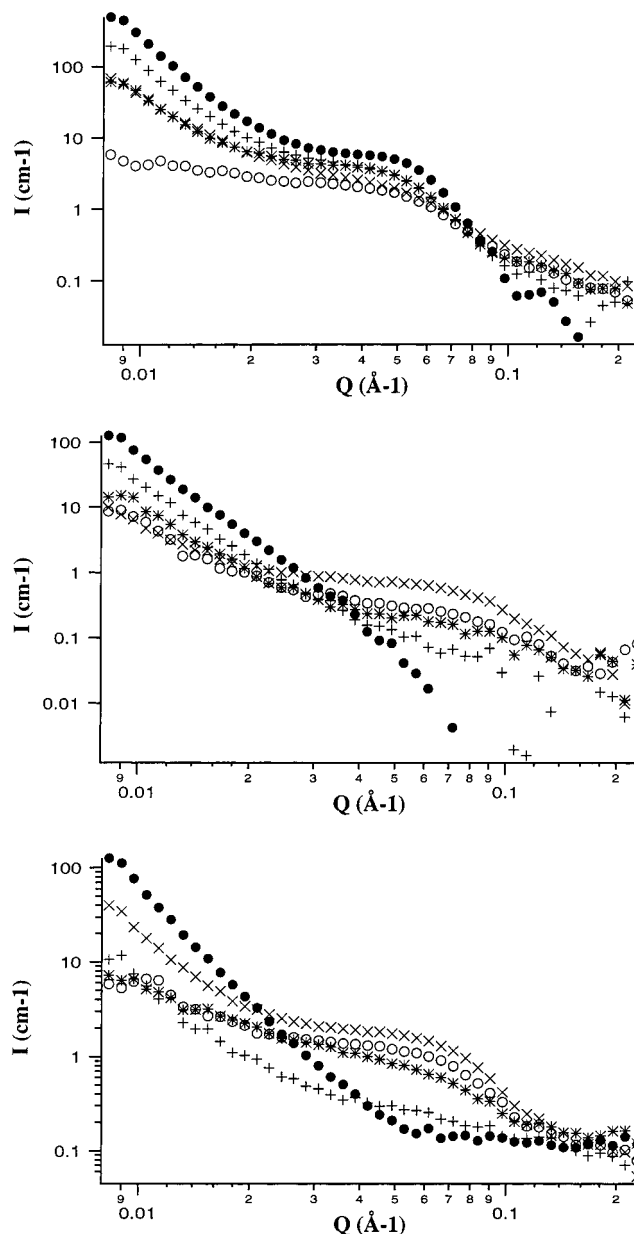


Figure 2. Small-angle neutron scattering for three emulsions at 20 °C illustrating change with isotopic contrast: (a, top) H₂O–D₂O/E surfactant/C₁₆D₃₄ (●, 100% H₂O; +, 75% H₂O; *, 50% H₂O; ○, 25% H₂O); (b, middle) NH₄NO₃ + D₂O/E surfactant/C₁₆H₃₄–C₁₆D₃₄. (●, 100% C₁₆H₃₄; +, 68% C₁₆H₃₄; *, 53% C₁₆H₃₄; ○, 37% C₁₆H₃₄; ×, 0% C₁₆H₃₄); (c, bottom) NH₄NO₃ + D₂O/A surfactant/C₁₆H₃₄–C₁₆D₃₄. (●, 100% C₁₆H₃₄; +, 53% C₁₆H₃₄; *, 37% C₁₆H₃₄; ○, 21% C₁₆H₃₄; ×, 0% C₁₆H₃₄).

droplets and the microemulsion, a contribution from the microemulsion itself, and a flat background. Ravey et al.⁵⁵ have shown that a simple addition of intensities is appropriate, providing the relative curvatures of the microemulsion microstructure and the interface are sufficiently different. The various scattering models used are summarized below.

Uncorrelated Flat Interfaces.⁵⁶ For an interface of specific area A , consisting of an adsorbed layer of surfactant between

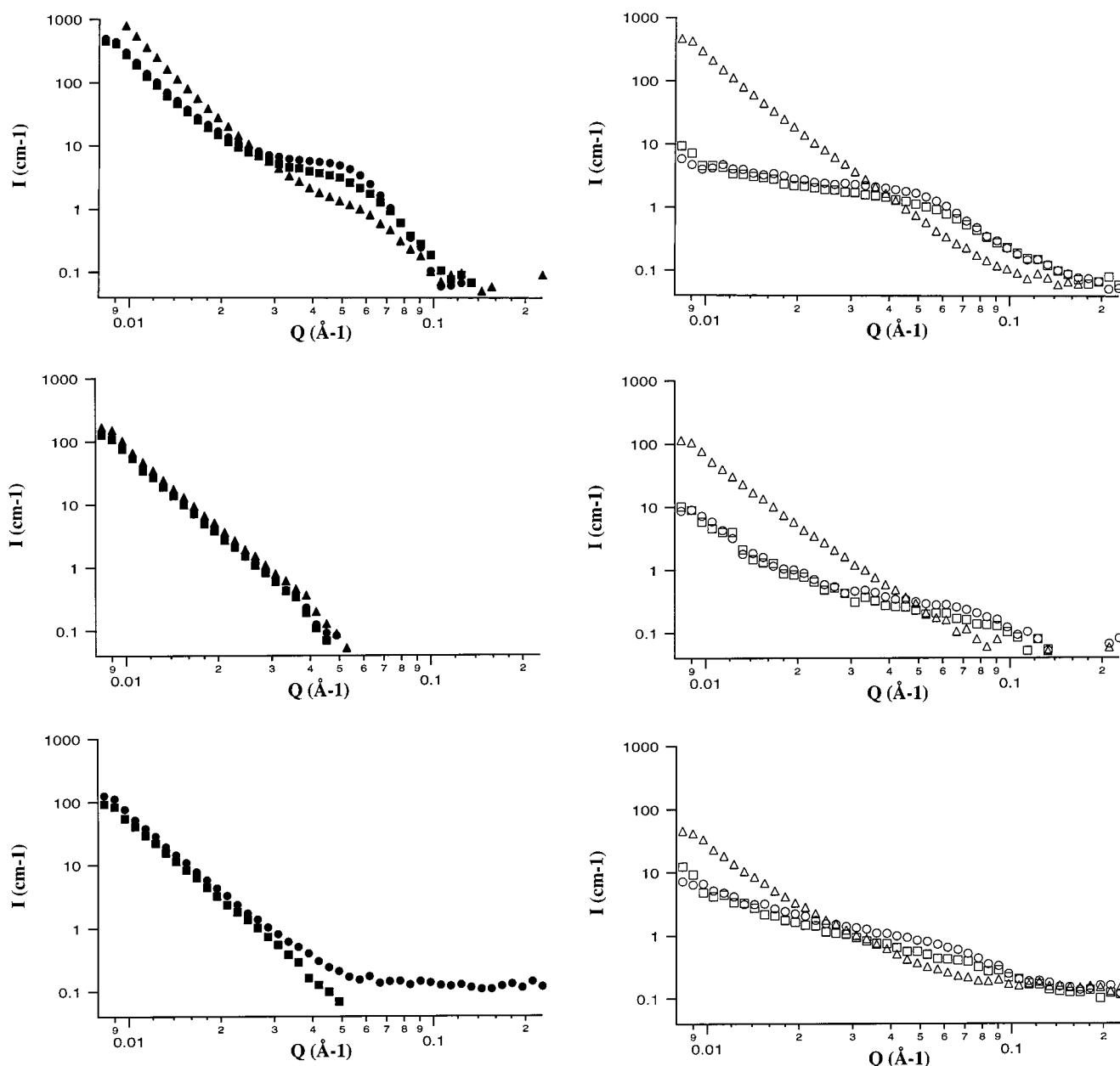


Figure 3. Temperature dependence of scattering data throughout (Δ) 5 °C data, (\circ) 20 °C, and (\square) 70–80 °C: (a, top) H_2O – D_2O /E surfactant/ $\text{C}_{16}\text{D}_{34}$, (i, left) 100% H_2O , (ii, right) 25% H_2O ; (b, middle) NH_4NO_3 + D_2O /E surfactant/ $\text{C}_{16}\text{H}_{34}$, (i, left) 100% $\text{C}_{16}\text{H}_{34}$, (ii, right) 37% $\text{C}_{16}\text{H}_{34}$; (c, bottom) NH_4NO_3 + D_2O /A surfactant/ $\text{C}_{16}\text{H}_{34}$, (i, left) 100% $\text{C}_{16}\text{H}_{34}$, (ii, right) 37% $\text{C}_{16}\text{H}_{34}$.

aqueous and hexadecane phases, we can write the intensity of scattering as

$$I(Q) = 2\pi A/Q^4[(\rho_a - \rho_{\text{me}})^2 + 4(\rho_a - \rho_s)(\rho_s - \rho_{\text{me}}) \sin^2(QT/2)] \quad (1)$$

where ρ_a is the scattering length density of the aqueous phase, ρ_s is that of the surfactant layer of thickness T , and ρ_{me} is the mean scattering density of the nonaqueous phase. This formula can be reduced to the usual Porod form for a step and the usual lamellar form, by use of appropriate scattering length densities.

This formula assumes that the interfaces are mutually uncorrelated; if they are, an extra multiplicative term $S(Q) \neq 1$ should be added as an initial approximation. At sufficiently high Q interparticle effects can be neglected and an analysis of the local structure can be attempted independent of the larger scale structure.^{10,43} Given that our minimum Q is 0.0037 \AA^{-1} , and

the droplets are micrometer-sized, we can neglect droplet–droplet correlation. We may however need to consider mutual alignment and preferred spacing of interfaces across the continuous oil-rich emulsion phase.

Correlated Spherical Micelles. The scattering from a polydisperse uniform hard sphere fluid, of mean radius r and sphere volume fraction ϕ in the Percus–Yevick approximation with a polydispersity given by the Schultz distribution, with a relative width σ , can be calculated exactly.⁵⁷ Ravey et al.^{27,29,58} find that the results are relatively insensitive to realistic values of a hard sphere stickiness parameter, so a nonsticky hard sphere is a realistic approximation. In addition to the micelle volume fraction and scattering length density difference from the continuous phase, the disposable parameters are only the micellar radius and polydispersity factor.

Correlated Rodlike Objects. A common rodlike morphology in surfactant solutions directly observed by cryo-TEM, as well

as inferred from rheology, light, X-ray, and neutron scattering, are long wormlike flexible curved micelles.^{14,43,59,60} The wormlike micelles convolve, while self-avoiding, into a large-scale globular structure, rather resembling that observed in dilute solutions of polymers. The form factor for an individual micelle can be calculated by use of an analytical fit to a Monte Carlo simulation of this structure.^{61–63} This fit is valid not only for highly convoluted long worms, but down into a range in which the worms are quite short. The specific disposable parameters are the cylindrical cross-sectional radius, the total cylinder length, and the cylinder persistence length—a measure of the worm flexibility or curvature, and the worm-length Schultz polydispersity. This theory neglects the excluded volume effect within the micelle. However, this is not important within a micelle for ratios of worm length to persistence lengths of less than about 25.^{59,63} At higher surfactant volume fractions, however, intermicellar correlation will become important in the range of Q of our SANS data, especially for shorter worm lengths. We correct for this by calculating $S(Q)$ assuming that the micelles are composed of spheres, as above, with an external radius given by multiplying the radius of gyration already given by the worm theory by $(5/3)^{1/2}$. This introduces no extra parameter.

Correlated Lamellae. Although there is extensive literature on the scattering from lamellar phases,^{8–12,38,39,64–66} no model for swollen lamellar phases is valid for our SANS data over the entire Q range and at our concentrations. The model of Porte et al.⁶⁶ involves elastic thermal deformation of an ordered swollen lamellar arrangement by both bending of lamellae and variation of interlamellar distance. This shows a transition from Bragg-like scattering to smooth, small-angle scattering, as the lamellae become less laterally rigid. It neglects excluded volume effects due to the van der Waals volumes of the lamellae, which at our surfactant volume fraction of ca. 0.2 are bound to be significant. The functional form of the Landau expansion of Teubner and Strey³⁸ requires an observable maximum in $I(Q)$, and thus is valid only when there is more lamellar order than is qualitatively apparent for our system.

Uncorrelated lamellae have been shown to fit higher Q data in a lamellar system,¹⁰ so an approximation due to Debye^{67–69} has been chosen for the scattering from dilute lamellae:

$$S(Q) = 1 - 2\phi_{\text{lam}}(\sin Qd_{\text{excl}}/(Qd_{\text{excl}})) \quad (2)$$

where ϕ_{lam} is the volume fraction of the lamellar van der Waals volume (which may be greater than the surfactant volume fraction given some incorporation of hexadecane) and d_{excl} is a distance within which no other lamella may approach. This model posits a one-dimensional gas of lamellae, with a characteristic excluded volume around each lamella. The lamellae thus have short-range, but no long-range, order.

Results

Figure 2 shows the SANS data at 20 °C for the three emulsions studied. Noticing that this figure shows data over three decades of intensity, we can see there is much to interpret. There is a “bump” at Q of ca. 0.06 \AA^{-1} in many plots, but its intensity also varies, and it is indeed sometimes absent. It is clear by inspection that no single one of the models above will be adequate to describe this variety of data.

Qualitative Description at 20 °C. There are three extreme contrasted types of emulsions that can be assembled with hydrogenous surfactants: (a) deuterated aqueous phase/hydrogenous surfactant/hydrogenous hexadecane (DHH), (b)

deuterated aqueous phase/hydrogenous surfactant/deuterated hexadecane (DHD), (c) hydrogenous aqueous phase/hydrogenous surfactant/deuterated hexadecane (HHD).

Since the scattering length densities of hydrogenous surfactant, H_2O , and $\text{C}_{16}\text{H}_{34}$ are similar, and very different from those of D_2O and $\text{C}_{16}\text{D}_{34}$, which are almost the same, the SANS from these systems can be interpreted as follows. DHH will define the boundary(ies) between the aqueous phase and the hexadecane and surfactant—without distinguishing between the latter if their individual SLDs are almost the same—which they are when fully hydrogenous (Table 1). DHD will highlight the surfactant distribution, without distinguishing the aqueous phase from hexadecane—provided the deuterations of hexadecane and the aqueous phase are adjusted such that their SLDs are the same. Last HHD will highlight hexadecane—again since SLDs for the surfactant and H_2O are very similar.

(1) DHH reveals the aqueous/oil interface *and* any scattering from surfactant in the aqueous droplets *and* any water in the oil phase.

(2) DHD reveals *only* surfactant structures in the oil and water and at the interface.

(3) HHD reveals the aqueous/oil interface *and* surfactant plus water scattering from structures in the oil phase.

If we examine Figure 2a, we see a smooth transition from HHD (filled circles) to DHD (open circles). We notice that at small Q the initial ca. Q^{-4} dependent scattering collapses 2 orders of magnitude as we go from HHD to DHD. This reflects the contrast matching of strong scattering from the droplet/oil interface, which dominates in HHD at low Q . However, at higher Q the “bump” structure changes, but not so dramatically. This indicates that there is surfactant structure in the oil phase but *none* in the aqueous phase. This structure is small scale and dominates the Porod scattering at these higher Q values.

In Figure 2b,c the transition is from DHH (filled circles) to DHD at intermediate contrasts and then partway to HHD for the $\text{C}_{16}\text{D}_{34}$ emulsion (X points). This is because the ammonium nitrate aqueous phase is partly hydrogenous and has an SLD of 3.52 compared to $6.74 \times 10^{10} \text{ cm}^{-2}$ for hexadecane- d_{34} . However, we notice the lack of microstructure at high Q for the DHH, confirming that there is insignificant microstructure due to surfactant in the aqueous phase and only small scattering due to water in the oil phase. Again the interface scattering is strong at low Q when oil + surfactant strongly contrasts the aqueous phase.

These results qualitatively confirm our expectation that we are observing the sum of SANS from the aqueous oil interface and from surfactant microstructure in the oil phase. The alternative of finely divided surfactant can be eliminated since significant Porod scattering would be observed from the surfactant/emulsion interfaces, as we shall see in the 5 °C data. We will now proceed to quantitative analyses.

Contrast Match and Porod Plots at 20 °C. As we note above, the DHH system provides the scattering with the least oil-phase microstructure effects and which is most dominated by interface effects. Figure 4 shows a plot of $\ln(I(Q)Q^4)$ against Q^2 for this contrast (filled circles in Figure 2b) in the AN–E series. This plot is linear over the entire Q range; the bumps may not be significant on this expanded scale. Equation 1 shows that we expect this linear relationship if the interface between the aqueous phase and hexadecane plus surfactant (note $\rho_s = \rho_{\text{me}}$) is a flat surface, that is, we have Porod scattering. The degree of roughness can be estimated from the slope of this plot. We obtain a root-mean-square local roughness of $10(10) \text{ \AA}$ and a droplet surface area of $0.45(1) \text{ m}^2/\text{cm}^3$ of emulsion.

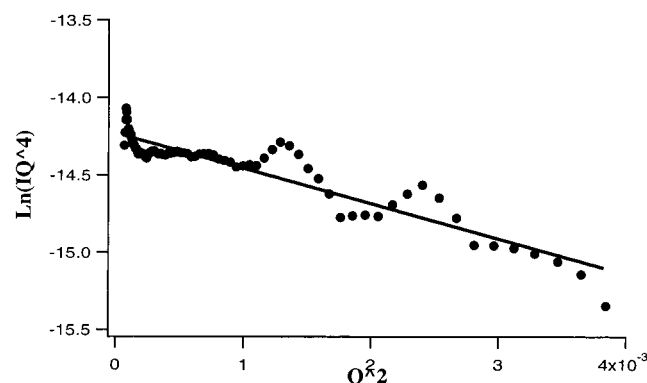


Figure 4. $\ln(I(Q)Q^4)$ versus Q^2 for aqueous ammonium nitrate plus D_2O phase/hydrogenous surfactant and hydrogenous hexadecane (DHH).

From the remainder of the data we obtain a roughness for the ammonium nitrate/E surfactant series at 80 °C of 10(10) Å, for the ammonium nitrate/A surfactant series 10(10) Å at 20 °C and 10(10) Å at 80 °C, and for the water/E surfactant series 60(20) Å at 20 °C and 50(15) Å at 80 °C.

This excellent series of Porod plots provides a number of strong constraints on the emulsion structure. There is no evidence of scattering from highly curved surfaces. In the Q range observed curvature from radii of less than ca. 600 Å would distort the linear plot. Given the micrometer-sized and rounded aqueous droplet sizes observed optically and by cryo-TEM, this is however not a surprise. Measurements by ultra-small-angle scattering might well detect this small curvature.

There is also no obvious scattering attributable to interference associated with the slab of hexadecane-rich material between the surface of adjacent droplets. If the aqueous/hexadecane interface of one droplet was within 800 Å of the hexadecane/aqueous interface of its neighbor across the hexadecane layer, and these distances, d_{bi} , were relatively constant between droplets, a slablike form factor or even interference fringes between them might be observed. We have used the formula $d_{bi} = 2\pi/\Delta Q$, where ΔQ is the best experimental resolution. An alternative explanation for the lack of a fringe structure is that the dispersion of d_{bi} is large, compared to $2\pi/\Delta Q$.

Thus, the hexadecane + surfactant layers between droplets either are relatively uniform and of thickness greater than 800 Å, or vary in thickness significantly between $2\pi/\Delta Q$ (max) \approx 31 Å and $2\pi/\Delta Q$ (max) = 800 Å. An older model that we can immediately exclude is a thin uniform bilayer of surfactant, ca. 30–100 Å thick, separating aqueous droplets, with the remainder of the surfactant and the hexadecane completely drained to the Plateau borders.

The linearity of similar Porod plots in the SAND data, and the smaller minimum Q of SAND compared to LOQ (0.0036 vs 0.008 Å⁻¹) and its improved resolution, extends this discussion of droplet–droplet hexadecane layer thickness. If there is a strong peak in the distribution of this hexadecane layer thickness in the emulsion, it must be at distances greater than 3000 Å. From the known emulsion composition, and mean aqueous droplet size, a uniform droplet distribution gives a calculated average oil thickness of ca. 1000 Å. This strongly suggests no strongly favored hexadecane thickness. We are thus led to the conclusion, independently of the cryo-TEM, that the hexadecane-rich layer is distributed around the droplets with a wide spread of droplet surface to droplet surface distances. A further constraint, relevant later, is that the degree of flatness of these plots from SAND and LOQ provides a strong constraint on the amount of water present within the hexadecane phase in

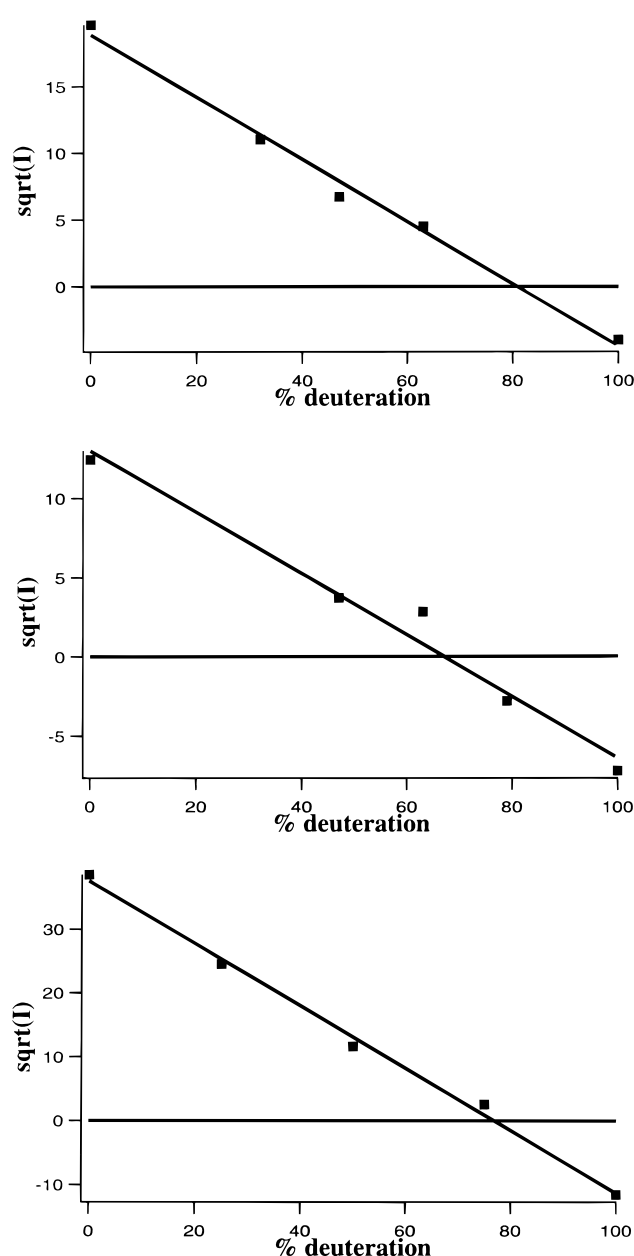


Figure 5. Contrast match plots of $\sqrt{I(Q)}$ at $Q = 0.008$ Å⁻¹ against mole percent deuteration for the series (a, top) $NH_4NO_3 + D_2O/E$ surfactant/ $C_{16}H_{34}-C_{16}D_{34}$, (b, middle) $NH_4NO_3 + D_2O/A$ surfactant/ $C_{16}H_{34}-C_{16}D_{34}$, and (c, bottom) H_2O-D_2O/E surfactant/ $C_{16}D_{34}$.

some organized form such as reverse micelles. Last, since the surfactant headgroup and tail have rather different scattering length densities, we should note that this plot implies that we are not able, in this Q region, to resolve any organized surfactant headgroup regions from tail regions.

If eq 1 describes the low- Q scattering, not only the Q dependence, but also the isotopic dependence, should be quantitatively described. We have plotted $\sqrt{I(Q)}$ at the minimum Q of 0.008 Å⁻¹ versus $C_{16}D_{34}$ mole fraction across our complete AN–E contrast series (Figure 5a). The good straight line found was as expected if our simple model of eq 1 is correct, with a contrast match point at 81(1)% deuteration of the oil phase. The straight line implies that any other scatterers in the system, when surfactant and oil are unmatched, have small scattering intensity at Q of 0.008 Å⁻¹, or that these scatterers are so polydisperse as not to contribute much to the intensity at the observed Q . This would imply inhomogeneities elsewhere on a

scale of 200 Å or less, given the Q scale. The contrast match point can be transformed, by use of Table 1 and the emulsion weight composition, into a measurement of the weight density of the ammonium nitrate aqueous phase of 1.46(2) gm cm⁻³, in good agreement with the direct measurement of bulk solution estimated by extrapolation as 1.40 gm cm⁻³ at 20 °C.

As for the AN-E system, we estimate aqueous-phase densities and interfacial surface areas from Figure 5b,c. The AN-A of Figure 5b gives a surface area of 0.45 m² cm⁻³ and an ammonium nitrate aqueous-phase density of 1.50(5) gm cm⁻³. The H₂O-E series of Figure 5c has a specific surface area of 0.78 m² cm⁻³ and a calculated aqueous-phase density of 1.08(1) gm cm⁻³ at the contrast match point. This agrees well with the density of 1.08 g cm⁻³ expected for the match point 75% deuterated water mixture.

For the AN-E series by chance no emulsion close to the match point was studied. However, for the AN-A series and the H₂O-E series there are emulsions studied close to the contrast match point. The former has a match point of 67(2)% deuteration, and we have studied a 63% emulsion (asterisk in Figure 2c), while for the latter we have a match point of 76-(1)% and have studied a 75% D₂O mixture (open circles in Figure 2a). For these two emulsions we have excellent data relating to the surfactant structures and distribution uncontaminated by scattering due to unbalance of aqueous and hexadecane SLDs. We shall however in the next section model these and the highly unmatched emulsions with a consistent model.

Correlated Spherical Micelle Fitting at 20 °C. Figure 6 shows the fits for each of the three emulsion series for data which are furthest and nearest to the contrast matched condition of each. The full lines are the model fits to the data. The full model contains a large number of parameters, so we have fixed many of these. In all cases we have assumed uniform reverse micelles, and ignored the probable presence of a water-rich structural core. Test calculations show that this affects the higher Q data only marginally. For the contrast unmatched data we have also fixed the radius and polydispersity of the reverse micelles at values found from the contrast matched data. Conversely we have fixed the interface roughness for the contrast matched data at the value found from the unmatched data. The refined values of scattering length densities and micellar volume fraction imply a particular chemical composition of the emulsion mix. Since this is already known, we have, by successive iteration of refinements, fixed the micellar volume fraction at a constant value consistent with both the known emulsion composition and the final refined values of scattering length densities which emerge from the fitting process. The resulting total nine-parameter model (including two flat backgrounds) has been fit to three pairs of experimental data. We have been unable to fix further parameters since doing so drastically degrades the fit. If the model is realistic, the derived values of these parameters should also be significant, and the values must be physically realistic—e.g., no negative volume fractions.

In Table 2 we have transformed the seven interesting parameters into seven physically transparent quantities associated with the emulsion. For the reverse microemulsion we list the radius and polydispersity of the spherical reverse micelles, and the water and hexadecane volume fraction in the micelles together with the surfactant content—which is fixed by the previous two fractions. We also note the micelle volume fraction in the hexadecane oil microemulsion that these values imply. For the aqueous/oil interface we list the area, the roughness, and the amount of surfactant adsorbed at the interface. We also

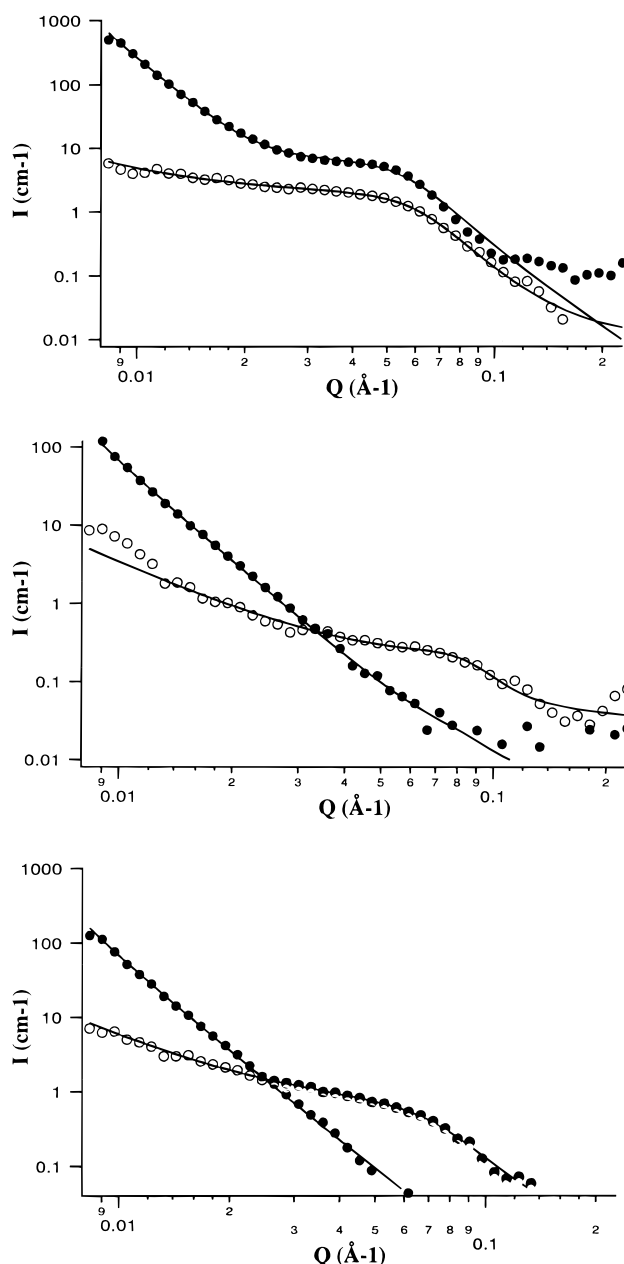


Figure 6. Comparison of the best spherical micelle plus interface scattering model with experiment (a, top) H₂O-D₂O/E surfactant/C₁₆D₃₄ (●, 100% H₂O; ○, 25% H₂O); (b, middle) NH₄NO₃ + D₂O/E surfactant/C₁₆H₃₄-C₁₆D₃₄ (●, 100% C₁₆H₃₄; ○, 37% C₁₆H₃₄); (c, bottom) NH₄NO₃ + D₂O/A surfactant/C₁₆H₃₄-C₁₆D₃₄ (●, 100% C₁₆H₃₄; ○, 37% C₁₆H₃₄). The full lines are the best fits to the data at the two contrasts.

list the resulting quantity and the weight fraction of the surfactant absorbed at the interface. For the H₂O-E emulsion the unbalanced emulsion showed significant micellar scattering, and we required variation of the micellar radius in these data as well. The table shows two entries for this emulsion, the first derived from the contrast matched data.

Correlated Lamellar and Rodlike Micelle Simulations at 20 °C. Although none of the quantities in Table 2 seem seriously anomalous, there are sufficient model parameters that might lead us to question the uniqueness of this model, and we will now proceed to show that these present data are indeed able to be fitted by two further different models. Figure 7 shows simulations of two models, in particular of a system of correlated lamellae (---) for the contrast matched SAND data for D₂O-

TABLE 2: Structural Parameters Derived from Fitting the Emulsion Data^a

	H ₂ O-E	AN-E	AN-A
microemulsion, micelle radius (Å)	33.7(6) 36.3(1)	30(2)	26(2)
micelle polydispersity	0.42(1)	0.26(4)	0.36(4)
water volume fraction in the micelle	0.24(1)	0.08(1)	0.10(1)
hexadecane volume fraction in the micelle	0.43(1)	0.57(1)	0.28(1)
surfactant volume fraction in the micelle	0.33	0.35	0.62
volume fraction of micelles in the oil phase	0.34	0.35	0.16
aqueous droplet/oil phase interface specific surface (m ² mL ⁻¹)	0.71(1)	0.58(1)	0.59(1)
interface roughness (Å)	62(1)	0(3)	0(3)
surfactant concentration absorbed at the interface (mg/m ²)	0.79(1)	1.7(1)	2.2(1)
fraction of the total surfactant absorbed at the interface	0.06	0.12	0.16

^a Errors are attached only to the seven values derived directly from the seven model parameters; other errors are derivable.

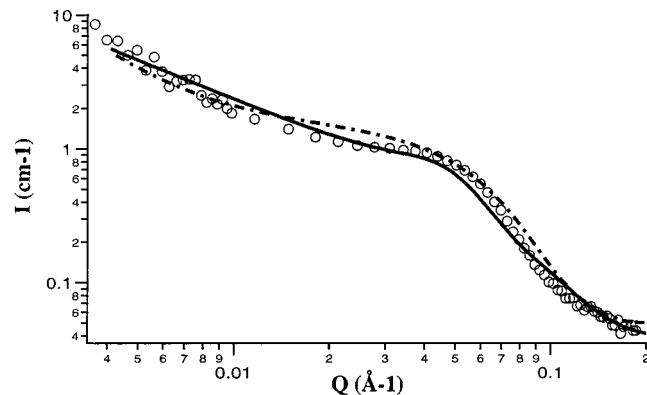


Figure 7. Simulation of H₂O-D₂O/E surfactant/C₁₆D₃₄: 25% H₂O SAND data, correlated lamellae (---), short worm model (—).

H₂O mixtures/E surfactant/C₁₆D₃₄, 25% H₂O. A model of short wormlike micelles (continuous line) fit the data nearly as well.

The rod model gives a very short rod length, of 200 Å, and a diameter of 32 Å, and a suggestion of significant flexibility shown by a persistence length of 50 Å. The rods are relatively flexible, giving extra disorganization, while the length is relatively short. These values are broadly similar to the results of Penfold et al. on Co(AOT) microemulsions.⁶ The lamellar model gives a 32 Å thick lamella, with an exclusion length of 65 Å and a ϕ_{excl} of 0.47(1). Neither model requires an interface scattering term, since at low Q both models have significant slopes, unlike the sphere model, and are thus capable of fitting low- Q data without an additional term. However, if an interface term similar to that of the sphere model is arbitrarily added, good fits are still obtainable. In the lamellar simulation we find a lamellar scattering length corresponding to a hexadecane content of 58(5)% by volume fraction; the flexible rod model gives 23(5)%. The surfactant microstructure, as for the spherical model, incorporates a significant amount of hexadecane.

The high- Q data force all the models to a characteristic short distance of about 50 Å—lamellar thickness or rod diameter; just as for the spheres we obtained a diameter of 50–70 Å. In all cases there is also a longer characteristic interparticle distance forcing the intensity at smaller Q downward—the 100 Å spherical intermicelle approach distance, a 200 Å worm length, and a 65 Å d_{excl} for the excluded lamellar volume. Thus, all models have a very broad agreement in featuring two characteristic length scales.

Temperature Dependence of the Data. On heating from 20 to 70–80 °C, the exact temperature depending on the particular sample, there are few changes in the small-angle scattering. Figure 3 shows that the interfacial scattering is almost invariant, while the scattering at higher Q , from the reverse microemulsion structure in the oil phase, changes in that the

bump at Q ca. 0.06 Å⁻¹ decreases only slightly in intensity. This is consistent with the scattering objects being in the nonbicontinuous single- or two-phase L₂ region.

On cooling the samples from 70–80 to 5 °C, which was the experimental procedure, there are gross changes. Wherever there was a high- Q bump, it has almost or entirely disappeared. Conversely the intensity of scattering, which is linear in $\ln(I(Q))$ versus $\ln(Q)$, has in all cases increased. This is most dramatically seen in Figure 3a(i). A reversible re-entry to the bicontinuous L₂ or L_α phase region appears to be excluded.

The 5 °C intensity data for all the plots decrease in intensity at a Q dependence of close to Q^{-4} . This means that all the scattering objects in the emulsions are now flat on the scale of our experimental resolution of ca. 600 Å. That is, none of our scattering objects now contain microstructure. The freezing point of pure hexadecane is 18.1 °C, and the freezing point of the aqueous droplets is 4 °C for D₂O—or even less for other aqueous mixtures. It is known that these emulsions do not crystallize ammonium nitrate on cooling to -40 °C, and so scattering from the surface of ammonium nitrate microcrystals is probably excluded.

At 5 °C we probably then have fluid aqueous droplets separated by a very viscous or solid hexadecane—surfactant region. Since this latter region no longer contains the surfactant microstructure, it is likely that phase separation has occurred between a surfactant-rich phase and a hexadecane-rich phase. The specific surface areas for the three interfaces aqueous/hexadecane, hexadecane/surfactant, and aqueous/surfactant can be determined from a single contrast variation series (eq 1 with $T = 0$). $I(Q)$ varies quadratically in the deuterium content.

The H₂O-E series illustrates what is happening. Figure 3a shows a strong increase in scattering at 5 °C for both 100% H₂O and 75% D₂O. This strong increase for both can be interpreted as a separation of surfactant (SLD ca. 0) from C₁₆D₃₄ (SLD 6.74), the surfactant remaining within the hexadecane phase. If significant surfactant were to appear in the aqueous phase, there would be a much stronger dependence on the H₂O/D₂O ratio than is observed. If the water volume fraction in the separated surfactant-rich phase is about 20%, the same value that we have found for the reverse micelles, then we predict the ratio of the scattering length densities to be 63%. The agreement with the observed value of 53% is very good, as it is for intermediate deuterations. We conclude that the specific areas are 0.71 m² cm⁻³ for the aqueous/hexadecane, 1.20(5) m² cm⁻³ for the surfactant/hexadecane, and 0.0(1) m² cm⁻³ for the aqueous/surfactant interface.

The AN-E and AN-A series can be analyzed in a similar way, and we obtain for the three areas, respectively, 0.58, 0.50(5), and 0.22(3) m² cm⁻³ and 0.59, 0.03(1), and 0.17(2) m² cm⁻³. It has been necessary to invoke a nonzero surfactant/

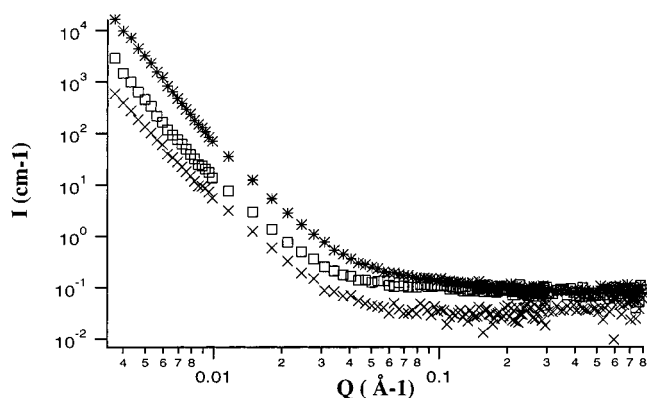


Figure 8. Preparation dependence of emulsions, SAND data: *, 30 s plus 2 min more effective (>500 rpm) stir; □, 30 s (ca. 250 rpm) plus 5 min of extra stirring (ca. 500 rpm); ×, 30 s (ca. 250 rpm) plus 2 min of extra stirring (ca. 500 rpm).

aqueous interface. A last point to notice is that the relative straightness of all the Porod plots eliminates the possibility that surfactant or other layers thicker than about 20 Å decorate any of the interfaces. On scales in our Q range all the interfaces are both flat and sharp.

Effect of the Stirring Procedure. Figure 8 shows three calcium nitrate samples of identical composition, but different emulsification history. These three samples scatter from the aqueous/hexadecane + surfactant interface—as for the DHH sample. We obtain specific surface areas of 0.25, 0.70, and 3.9 $\text{m}^2 \text{mL}^{-1}$, respectively, for (a), (b), and (c). This change reflects well the relative stirring effectiveness in the emulsification process.

Discussion

Nature of the Emulsions at 20 °C. The absolute intensity and its dependence on deuteration can be calculated for all of our data using a model whose characteristics are (1) interfacial scattering among water droplets, the oil phase, and surfactant absorbed at the interface, (2) a separation of the water–water interfaces by an oil phase averaging 1000 Å thick but very variable, (3) scattering from an assembled microstructure in the oil phase, and (4) the microstructure well modeled by any of the spherical inverse micelles, swollen lamellae, or rodlike micelles.

Aqueous/Oil Interface at 20 °C. The scattering at low Q from a flat interface between the large emulsion droplets and the hexadecane phase, in those cases when oil and water phases are not matched in SLD, shows no evidence of interdroplet interference—and in the SAND, data are sensitive to distances of up to 2000 Å. Therefore, the hexadecane phase, separating aqueous droplets, has a very wide distribution of thicknesses. Given an average droplet size of micrometers, the relative proportions of hexadecane and aqueous phases allow the hexadecane thickness to be estimated as about 1000 Å for a regular droplet distribution. We would thus expect to see interference effects if the hexadecane layer were evenly distributed. We can also eliminate a simple model in which hexadecane drains to Plateau borders, leaving a bilayer of surfactant separating aqueous droplets. We are left with the alternative that there is a wide distribution of hexadecane layer thicknesses varying over a great part of the distances 0–3000 Å. The interface has no significant regions of high curvature such as Plateau borders, smaller than a radius of about 600 Å. These observations are entirely consistent with the cryo-TEM observation of a hexadecane region with boundaries of curvature

similar to the droplet size. The hexadecane region occupies the interstices of a polydisperse close-packed system of spherical aqueous droplets, as in other high internal phase emulsions.²⁹ Other inhomogeneities within the emulsion giving rise to SANS are on a scale distinctly shorter than 200 Å.

The interfaces do not have a significant temperature dependence in the local roughness. The roughness for all the ammonium nitrate materials is close to 0 Å, while the water ones give about 60 Å. This is somewhat rougher than typical liquid/air interfaces, but is less than the 80–90 Å found for the surfactant-decorated decane/water interface.^{70,71} We can rationalize the difference between salt and water emulsions by noting that the weight density change across the interface is much more for the salt system, and we would expect this increase to suppress thermally driven fluctuations. In addition we notice that there is much more surfactant at the salt/oil interface than at the water/oil interface. This would also suppress local roughness by an increase in interfacial tension.

Only a small fraction of the total surfactant is present at the aqueous/oil interface—only 6% in the salt-free emulsion. Given the ionic nature of the acid amide headgroup, the larger value of 12–16% at the salt/oil interface might be expected for electrostatic reasons. These values correspond to an area per surfactant molecule of 230 Å² for the water emulsion and 83–110 Å² for the ammonium nitrate emulsions.

The tail thickness of this surfactant spread at the air/water interface measured by neutron reflectometry varies from about 15 to 20 Å.⁷² The fully extended tail is of length ca. 45 Å. Langmuir isotherms of this surfactant spread at the air/water interface give headgroup areas of 80–110 Å².⁷² This is also consistent with an estimated molecular volume of ca. 1500 Å³ from the physical density. We can then conclude that at the salt/oil interface we also have a similar close-packed monolayer of surfactant with the PIB tail not fully extended. The surfactant at the water/oil interface appears to be less than a monolayer.

The specific surface areas appear to be rather insensitive to deuteration, as we would demand, but are also not highly sensitive to salt content. The pure water system has a specific surface area only a little larger than that for both of the salt-containing aqueous phases studied. The specific surface areas obtained from these same samples optically, using a Malvern Mastersizer,²⁸ of 0.6–0.9 $\text{m}^2 \text{mL}^{-1}$ agree well with the SANS estimates. However, the mixing protocol has a much larger effect. The calcium nitrate emulsions prepared in different ways have surface areas which vary by a factor of 10.

Oil-Phase Microstructure at 20 °C. A good fit to the data is provided by a spherical, reverse micellar structure for the oil phase. Concerning the choice among lamellae, rods, and spheres, our discussion of previous work on microemulsions in the Introduction suggests a preference for a rod or sphere model. Contrariwise, one reason for attraction to a lamellar model for the structure is that we know from the DHH data that the surfactant-lined oil/aqueous interface is very flat. An obvious microstructure grown from this flat surfactant arrangement is lamellar, oriented parallel to the oil/aqueous interface. Dielectric measurements on our emulsions indicate that the surfactant molecules are clustered head-to-head,²⁸ but this is true of any of our models for the bulk of the surfactant. We shall confine our discussion to the spherical results, since we shall demonstrate that this is the correct model in a later paper.⁷²

The surfactant micellar structures for all emulsions contain significant hexadecane content—up to 57(1)%. Given the chemical similarity of *n*-alkyl and PIB chains, this mixing is not surprising. The water content of the surfactant structures is

24(1)% by volume in the H₂O–E emulsions. This corresponds to about 40 water molecules per surfactant molecule. For the AN emulsions the corresponding figure is 10–14 molecules. The latter corresponds to the values observed in lecithin-based reversed microemulsions—a molecule with a similarly complex headgroup,⁶⁰ and corresponds to about the number of primary ligating waters expected around our headgroup containing carboxylic acid, amide, and hydroxy groups. The higher water content of the micelles in the water emulsion correlates well with the greater roughness and larger headgroup areas observed at its aqueous/oil interface. The effect of added salt is not only to bind the surfactant more strongly at the aqueous/oil interface but also to reduce the availability of water to the micelles in the oil phase.

The higher water content of the aqueous emulsion is also reflected in the larger mean size of the micelles. If we assume the water comprises a central core, then the water content of 24% gives a central core of radius 22 Å surrounded by a hydrophobic shell of 13 Å thickness for the water emulsion. The salt emulsion water content of 8–10% gives 12 and 16 Å for the salt emulsions. The hydrophobic shell thicknesses are again similar to the surfactant tail lengths observed by reflectometry at the air/water interface.

Data are now also available for series varying surfactant concentration and aqueous concentrations, with variation of surfactant molecular weight.⁷² Previous SANS experiments have interpreted different data equally well as oblate² or prolate⁶ objects, while we have fitted these current data about equally well to both. However, these dilution experiments using more monodisperse surfactant, to be reported in a subsequent paper, show that in most regimes the oil phase consists of spherical reverse micelles. SANS studies of microemulsions assembled so as to mimic the oil phase in our emulsions confirm these conclusions.⁷²

Temperature Dependence of Emulsion Structure. The data at 70–80 °C are hardly different from those at 20 °C; the only noticeable effect is some small loss of structure in the hexadecane/surfactant high-*Q* region. This lack of temperature dependence over an extended temperature range is evidence for an oil phase of reverse micellar spheres, since lamellar or rodlike microemulsions are characteristically much more sensitive to temperature in their structural behavior.

However, at 5 °C all plots collapse to approximately Porod Q^{-4} plots. We have shown that the isotopic dependence is consistent with three approximately flat, approximately sharp interfaces—aqueous/hexadecane, hexadecane/surfactant, and aqueous/surfactant. A simple aggregation of a surfactant-rich phase as the hexadecane freezes could explain this. For the H₂O–E series these three interfaces have specific surface areas of 0.7, 1.20(5), and 0.0(1) m² cm⁻³ of emulsion, respectively. Given the surfactant volume fraction of 0.011 cm³ cm⁻³ of emulsion we can derive a large particle radius for the surfactant-rich aggregate of ca. 300 Å diameter. The particles are assumed spherical. The zero value for the aqueous/surfactant area implies that these particles reside in the hexadecane part of the emulsion. For AN–E the areas of 0.58, 0.50(5), and 0.22(3) m² cm⁻³ and the concentration of surfactant of ca. 0.012 cm³ cm⁻³ give a particle radius of ca. 500 Å and a significant intrusion of surfactant particles into the aqueous region. For the AN–A series this is more so. The areas of 0.59, 0.03(1), and 0.17(2) m² cm⁻³ and the surfactant concentration of surfactant of 0.011 cm³ cm⁻³ of emulsion give a particle radius of ca. 1600 Å, almost all of which lies in the aqueous region.

These numbers are consistent with the emulsion structure already deduced. The 20 °C data—and indeed the 5 °C data—preclude hexadecane/aqueous interfaces of a preferred thickness. There is a wide distribution in thicknesses occupying a significant fraction of the interdroplet region between 0 and 3000 Å. We also can calculate, from the average aqueous droplet size observed optically and the composition of the emulsion, that the average hexadecane thickness is ca. 1000 Å. This corresponds well with the surfactant particle sizes observed above: a 600 Å diameter can be contained within the hexadecane layer, 1000 Å intrudes a small amount—30(10)% of its surface—into the aqueous phase, and a 3200 Å diameter is 85–(5)% in the aqueous region, remembering that the aqueous region occupies 90% of the emulsion volume. If we assume our surfactant particle maximizes its immersion in the hexadecane layer, by having that layer as an equatorial belt, we can derive an average hexadecane thickness of 500(150) Å.

The last point is why the surfactant aggregated particles vary in size so much from series to series. We notice that the two E surfactants have similar surfactant-rich aggregate sizes at 300 and 500 Å radius, while the A surfactant gives 1600 Å. All have been subjected to similar cooling regimes. It may be that the purer A surfactant separates much better than the more mixed E surfactant.

Conclusion

We have examined by SANS three isotopically varying series of 90% internal phase water-in-oil emulsions whose aqueous droplets are several micrometers in diameter. We find that the SANS can be modeled by the sum of scattering from the aqueous droplet/oil interface and scattering from an oil-phase microemulsion of quite polydisperse reverse spherical micelles. We observe only a small fraction of the surfactant adsorbed at the interface. The majority is in the micelles, which also contain significant amounts of water and oil. The interfacial roughness, micellar size, and micellar water content all increase as we change from a salt-rich to salt-free aqueous phase. On heating from 20 to 70–80 °C the structure changes little, but on cooling to 5 °C surfactant aggregates 600–3200 Å in diameter are precipitated.

Although spherical micelles are the most likely oil-phase microstructure, these present data fit both lamellar and wormlike structures as well. We will present further SANS dilution experiments in a subsequent paper showing most, but not all, of these emulsions and related microemulsions contain spherical micelles.

These results complement those of Staples et al.⁴ who have just independently reached many similar conclusions, but on dilute internal phase oil-in-water emulsions with rather different surfactants. This suggests that these structures are common to most emulsions whether concentrated or not, independent of surfactant, whether O/W or W/O.

Acknowledgment. We thank Dr. P. Thiyagarajan and Mr. D. Wozniak at Argonne National Laboratory and Drs. R. Heenan and S. King at the Rutherford-Appleton Laboratory, U.K., for experimental assistance and advice on modeling, Dr. K. Edler of Bath University, U.K., for useful discussions, and Dr. S. R. Kline of NIST for supplying the first version of the IGOR fitting procedure. This work has benefited from the use of the Intense Pulsed Neutron Source at Argonne National Laboratory which is funded by the U.S. Department of Energy, BES-Materials Science, under Contract W-31-109-ENG-38. Travel grants through the Australian Government ISTAC/ANSTO Access to

Major Facilities Program are gratefully acknowledged. This work was financed by the Australian Research Council under SPIRT and SRF awards joint with ORICA and ICI UK Ltd. We also thank Dr. Deane Tunaley and Mr. Michael Bonadio of ORICA Pty. Ltd. for devising the method for small-scale emulsion preparation and Dr. D. E. Yates for useful discussions.

References and Notes

- (1) Cameron, N. R.; Sherrington, D.C. *Adv. Polym. Sci.* **1996**, *126*, 163.
- (2) Solans, C.; Pons, R.; Zhu, S.; Davis, H. T.; Evans, D. F.; Nakamura, K.; Kunieda, H. *Langmuir* **1993**, *9*, 1479.
- (3) Langenfeld, A.; Lequeux, F.; Stebe, M. J.; Schmitt, V. *Langmuir* **1998**, *14*, 6030.
- (4) Staples, E.; Penfold, J.; Tucker, I. *J. Phys. Chem. B* **2000**, *104*, 606.
- (5) Eastoe, J.; Steytler, D. C.; Robinson, B. H.; Heenan, R. K.; North, A. N.; Dore, J. C. *J. Chem. Soc., Faraday Trans.* **1994**, *90*, 2479.
- (6) Penfold, J.; Staples, E.; Tucker, I.; Cummins, P. *J. Colloid Interface Sci.* **1997**, *185*, 424.
- (7) Taisne, L.; Cabane, B. *Langmuir* **1998**, *14*, 4744.
- (8) Hornfeck, U.; Gradzielski, M.; Mortensen, K.; Thunig, C.; Platz, G. *Langmuir* **1998**, *14*, 2958.
- (9) Douglas, C. B.; Kaler, E. W. *J. Chem. Soc., Faraday Trans.* **1994**, *90*, 471.
- (10) Gazeau, D.; Bellocq, A.M.; Roux, D.; Zemb, T. *Europhys. Lett.* **1989**, *9*, 447.
- (11) Magid, L.; Butler, P.; Payne, K.; Strey, R. *J. Appl. Crystallogr.* **1988**, *21*, 832.
- (12) Strey, R.; Winkler, J.; Magid, L. *J. Phys. Chem.* **1991**, *95*, 7502.
- (13) von Berlepsch, H.; Keiderling, U.; Schnablegger, H. *Langmuir* **1998**, *14*, 7403.
- (14) Schurtenberger, P.; Scartazzini, R.; Magid, L. J.; Leser, M. E.; Luisi, P. L. *J. Phys. Chem.* **1990**, *94*, 3695.
- (15) Terech, P.; Schafhauser, V.; Maldivi, P.; Geunet, J. M. *Europhys. Lett.* **1992**, *17*, 515.
- (16) Eastoe, J.; Heenan, R. K. *J. Chem. Soc., Faraday Trans.* **1994**, *90*, 487.
- (17) Petit, C.; Lixon, P.; Pileni, M. P. *Langmuir* **1991**, *7*, 2620.
- (18) Eastoe, J.; Robinson, B. H.; Fragneto, G.; Towey, T. F.; Heenan, R. K.; Leng, F. *J. Chem. Soc., Faraday Trans.* **1990**, *86*, 2883.
- (19) Eastoe, J.; Robinson, B. H.; Williams, J.; Towey, T. F.; Heenan, R. K. *J. Phys. Chem.* **1993**, *97*, 1459.
- (20) Eastoe, J.; Robinson, B. H.; Heenan, R. K. *Langmuir* **1993**, *9*, 2820.
- (21) Lee, D. D.; Chen, S.H. *Phys. Rev. Lett.* **1994**, *73*, 106.
- (22) Lee, D. D.; Chen, S.H. *Nuovo Cimento D* **1994**, *16*, 1357.
- (23) Dibiasio, A.; Cametti, C.; Codastefano, P.; Tartaglia, P.; Rouch, J.; Chen, S. H. *Phys. Rev. E* **1993**, *47*, 4258.
- (24) Nagao, M.; Seto, H.; Okuhara, D.; Okabayashi, H.; Takeda, T.; Hikosaka, M. *Physica B* **1997**, *241*, 970.
- (25) Kellay, H.; Binks, B. P.; Hendrikx, Y.; Lee, L.T.; Meunier, J. *Adv. Colloid Interface Sci.* **1994**, *49*, 85.
- (26) Ravey, J.C.; Stebe, M.J. *Physica B* **1989**, *156*, 394.
- (27) Ravey, J. C.; Stebe, M. J. *Prog. Colloid Polym. Sci.* **1990**, *82*, 218.
- (28) Internal reports from ICI and Orica Ltd.
- (29) Ravey, J. C.; Stebe, M. J.; Sauvage, S. *Colloids Surf., A* **1994**, *91*, 237.
- (30) Schmidt, F.; Schick, M. *Phys. Rev. E* **1993**, *48*, 1882.
- (31) Holyst, R.; Oswald, P. *J. Chem. Phys.* **1998**, *109*, 11051.
- (32) Barnes, I.S.; Hyde, S.T.; Ninham, B. W.; Derian, P.J.; Drifford, M.; Zemb, T. N. *J. Phys. Chem.* **1988**, *92*, 2286.
- (33) Merdas, A.; Gindre, M.; Ober, R.; Nicot, C.; Urbach, W.; Waks, M. *J. Phys. Chem.* **1996**, *100*, 15180.
- (34) Ghosh, S. K.; Komura, S.; Matsuba, J.; Seto, H.; Takeda, T.; Hikosaka, M. *Jpn. J. Appl. Phys.* **1998**, *37*, 919.
- (35) Fukuda, K.; Olsson, U.; Wurz, U. *Langmuir* **1994**, *10*, 3222.
- (36) Leaver, M. S.; Olsson, U.; Wennerstrom, H.; Strey, R.; Wurz, U. *J. Chem. Soc., Faraday Trans.* **1995**, *91*, 4269.
- (37) Zemb, T. N. *Colloids Surf., A* **1997**, *130*, 435.
- (38) Teubner, M.; Strey, R. *J. Chem. Phys.* **1987**, *87*, 3195.
- (39) Milner, S. T.; Safran, S. A.; Andelman, D.; Cates, M.E.; Roux, D. *J. Phys. (Paris)* **1988**, *49*, 1065.
- (40) Larche, F. C.; El Qebbaj, S.; Marignan, J. *J. Phys. Chem.* **1986**, *90*, 707.
- (41) De Gennes, P. G.; Taupin, C. *J. Phys. Chem.* **1982**, *86*, 2294.
- (42) Zemb, T.; Dubois, M.; Deme, B.; Gulik-Krzywicki, T. *Science* **1999**, *283*, 816.
- (43) Magid, L.J. *J. Phys. Chem. B* **1998**, *102*, 4064.
- (44) Ninham, B. W.; Chen, S. J.; Evans, D. F. *J. Phys. Chem.* **1984**, *88*, 5855.
- (45) Ninham, B. W.; Evans, D. F.; Mitchell, D. J.; Blum, F. D.; Pickup, S. *J. Phys. Chem.* **1986**, *90*, 842.
- (46) Cametti, C.; Codastefano, P.; Tarataglia, P.; Chen, S. H.; Rouch, J. *Phys. Rev. A* **1992**, *45*, R5358.
- (47) Zemb, T. N. *Colloids Surf., A* **1997**, *130*, 435.
- (48) Eicke, H. F.; Meier, W.; Hammerich, H. *Colloids Surf., A* **1996**, *118*, 141.
- (49) Heenan, R. K.; King, S. M. *International Seminar on Structural Investigations at Pulsed Neutron Sources*; Report Number E3-93-65; Joint Institute for Nuclear Research: Dubna, Russia, 1993; p 176.
- (50) Heenan, R.; King, S. In *ISIS User Guide*; Boland, B., Whapham, S., Eds.; ISIS, Rutherford Appleton Laboratory: Didcot, U.K., 1992.
- (51) Thiagarajan, P.; Urban, V.; Littrell, K.; Ku, C.; Wozniak, D. G.; Belch, H.; Vitt, R.; Toeller, J.; Leach, D.; Haumann, J. R.; Ostrowski, G. E.; Donley, L. I.; Hammonds, J.; Carpenter, J. M.; Crawford, R. K. ICANS XIV—The Fourteenth Meeting of the International Collaboration on Advanced Neutron Sources, June 14–19, 1998, Starved Rock Lodge, Utica, IL; Vol. 2, pp 864–878.
- (52) IGOR Pro, Wavemetrics Inc., P.O. Box 2088, Lake Oswego, OR 97035.
- (53) Kline, S. R. Private communication.
- (54) Heenan, R. K.; King, S. M. Private communication.
- (55) Ravey, J.C.; Sauvage, S.; Stebe, M. J. *J. Phys. IV C8* **1993**, *3*, 141.
- (56) *Small Angle X-ray Scattering*; Glatter, O., Kratky, O., Eds.; Academic Press: London, 1982; p 17.
- (57) Griffith, W. L. *Phys. Rev. A* **1987**, *35*, 2200.
- (58) Ravey, J. C.; Stebe, M.J.; Sauvage, S. *J. Chim. Phys. Phys.-Chim. Biol.* **1994**, *91*, 259.
- (59) Pedersen, J.S.; Egelhaaf, S.U.; Schurtenberger, P. *J. Phys. Chem.* **1995**, *99*, 1299.
- (60) Schurtenberger, P.; Cavaco, C. *Langmuir* **1994**, *10*, 100.
- (61) Pedersen, J.S.; Laso, M.; Schurtenberger, P. *Phys. Rev. E* **1996**, *54*, R5917.
- (62) Pedersen, J. S.; Schurtenberger, P. *Macromolecules* **1996**, *29*, 7602.
- (63) Fujita, H. *Macromolecules* **1988**, *21*, 179.
- (64) Roux, D.; Coulon, C.; Cates, M.E. *J. Phys. Chem.* **1992**, *96*, 4174.
- (65) Teubner, M. *J. Chem. Phys.* **1990**, *92*, 4501.
- (66) Porte, G.; Marignan, J.; Bassereau, P.; May, R. *Europhys. Lett.* **1988**, *7*, 713.
- (67) Debye, P. *Phys. Z.* **1930**, *31*, 348.
- (68) Debye, P. *Phys. Z.* **1927**, *28*, 135.
- (69) Debye, P.; Menke, H. *Ergeb. Tech. Roentgenkd.* **1931**, *2*, 1.
- (70) Lee, L. T.; Langevin, D.; Farnoux, B. *Phys. Rev. Lett.* **1991**, *67*, 2678.
- (71) McClain, B. R.; Lee, D. D.; Carvalho, B. L.; Mochrie, S. G. J.; Chen, S. H.; Litster, J. D. *Phys. Rev. Lett.* **1994**, *72*, 246.
- (72) Reynolds, P. A.; Gilbert, E. P.; White, J. W. To be published.